Contribution from the Departments of Chemistry, North Carolina State University, Raleigh, North Carolina 27695, and The University of North Carolina at Charlotte, Charlotte, North Carolina 28223

Redox and Spectral Properties of Cobalt(II) and Copper(II) Tetraazaannulene Complexes: $\{H_2[Me_4(RBzo)_2[14]tetraeneN_4]\}$ (R = H, CO_2CH_3). Evidence for Superoxide Ligation and Reduction

Cynthia L. Bailey,[†] Robert D. Bereman,*[†] and D. Paul Rillema*[‡]

Received January 16, 1986

The electrochemical, spectral, and chemical properties of a series of Cu(II) and Co(II) tetraazaannulene complexes of the ligand $[Me_4(RBzo)_2[14]tetraeneN_4]^{2-}$ (R = H, CO_2CH_3) were investigated. The copper complexes each had two *irreversible* oxidation peaks centered at 0.37 and 0.87 V for R = H and at 0.54 and 1.05 V for R = CO_2CH_3, whereas the cobalt(II) complexes each exhibited three *reversible* oxidations at 0.01, 0.55, and 1.04 V for R = H and at 0.05, 0.67, and 1.21 V vs. SCCE for R = CO_2CH_3. The reduction values of the copper(II) complexes were −1.39 V for R = H and −1.17 V vs. SSCE for R = CO_2CH_3. The $E_{1/2}$ values for the reduction of the cobalt complexes were −1.65 V for R = H and −1.45 V for R = CO_2CH_3. A linear relationship in the difference in redox potentials between the first ligand oxidation and metal-centered reduction and the energy of the first visible transition suggested this band should be assigned as a ligand to metal charge transfer. Oxidation of the cobalt complex (R = H) by controlled-potential electrolysis resulted in an absorbance shift of the visible band from 16.8×10^3 to 18.4×10^3 cm^{-1} after removal of the first electron and to 18.5×10^3 cm^{-1} after removal of the second electron. The second oxidation product exhibited an isotropic ESR spectrum with $g = 2.0027$ (±0.003). Oxidation of the copper complex (R = H) resulted in formation of a copper(II) ligand coupled dimer, which exhibited an ESR signal with $g_\parallel = 2.149$ (±0.002) and $g_\perp = 2.045$ (±0.002). Electrolytic reduction of the copper complex (R = H) resulted in loss of the visible absorption band at 15.6×10^3 cm^{-1}, whereas reduction of the cobalt analogue resulted in a shift of the visible band from 16.8 to 15.9×10^3 cm^{-1}. The five-coordinate $Co[Me_4(CO_2CH_3Bzo)_2[14]tetraeneN_4]\cdot py$ complex gave ESR parameters of $g_\parallel = 2.208$ (±0.002), $g_\perp = 2.0021$ (±0.0003), and $A_\perp = 74.80$ (±0.5) $\times 10^{-4}$ cm^{-1}; the superoxide adduct that formed in the presence of O_2 and pyridine gave ESR parameters of $g_\parallel = 1.998$ (±0.002), $g_\perp = 2.086$ (±0.002), $A_\parallel = 8.95$ (±0.5) $\times 10^{-4}$ cm^{-1}, and $A_\perp = 18.7$ (±0.5) $\times 10^{-4}$ cm^{-1}. The coordination of the copper complex (R = H) with O_2^- was supported by the observation that the molar absorptivity of the visible band doubled upon stoichiometric addition of O_2^-. In addition, O_2 was reduced at a more favorable potential (70-mV shift) at a surface-modified electrode containing a polymer film of $Cu[Me_4Bzo_2[14]tetraeneN_4]$.

Introduction

Studies designed to characterize the interaction between substrates and metal centers in biological systems have long been of interest. One popular approach among inorganic chemists has been the design of metal complexes that mimic the properties of the active sites in metalloproteins. Over the last 10 years, our laboratories have carried out extensive studies of copper complexes that exhibit spectral and chemical properties similar to "type II" or "nonblue" copper(II).[1-5] We have now extended our investigation of metallo derivatives of the tetraazaannulene ligand shown in Figure 1 in an attempt to further understand the reactivity of the type II sites. This ligand system and its derivatives are particularly well suited as model compounds since they provide a stable N_4 environment whose coordination closely resembles that of porphyrin systems as well as that of nitrogen-coordinated amino acid transition-metal complexes. Proteins represented by these two areas include myoglobin, hemoglobin and copper–zinc superoxide dismutase.[6-15] The first two systems are involved in reversible dioxygen binding, while superoxide dismutase is proposed to play a role in the disproportionation of superoxide ion in living cells.

Previously we reported[16] the redox properties of a series of nickel(II) tetraazaannulenes based on the ligand depicted in Figure 1 and a surface-modified-electrode study[17] that involved characterization of electrodes which support thin films of oxidatively electropolymerized nickel(II) tetraazaannulene complexes. In the work reported here, the spectral, electrochemical and chemical properties of both cobalt(II) and copper(II) tetraazaannulenes are reported. Specifically, *n* values were determined by coulometry for a number of electrochemical processes, spectra of oxidized and reduced species as well as parent complexes were recorded, electronic absorption assignments were made on the basis of a model proposed by Lever and coworkers,[18] and the reaction of Co(II) complexes with O_2 to form $Co(III)-O_2^-$ complexes and the reaction of O_2^- with Cu(II) to form $Cu(II)-O_2^-$ complexes were investigated by electron spin resonance (ESR) and optical spectroscopy. In addition, the reactivity of O_2^- with electropolymerized films of the Cu(II) complex (R = H) was examined by using cyclic voltammetry.

Experimental Section

Materials. $Cu[Me_4Bzo_2[14]tetraeneN_4]$, $Cu[Me_4(CO_2CH_3Bzo)_2[14]tetraeneN_4]$, $Co[Me_4Bzo_2[14]tetraeneN_4]$, and $Co[Me_4(CO_2CH_3Bzo)_2[14]tetraeneN_4]$ were prepared by previously reported methods.[16,19] Elemental analyses were satisfactory in all cases and are

[†] North Carolina State University.
[‡] The University of North Carolina at Charlotte.

(1) Bereman, R. D.; Ettinger, M. J.; Kosman, D. J.; Kurland, R. J. *Adv. Chem. Ser.* **1977**, *No.* 162, 263.
(2) Giordano, R. S.; Bereman, R. D.; Kosman, D. J.; Ettinger, M. J. *J. Am. Chem. Soc.* **1974**, *96*, 1023.
(3) Giordano, R. S.; Bereman, R. D. *J. Am. Chem. Soc.* **1974**, *96*, 1019.
(4) Marwedel, B. J.; Kosman, D. J.; Bereman, R. D.; Kurland, R. J. *J. Am. Chem. Soc.* **1981**, *103*, 2842.
(5) Bereman, R. D.; Dorfman, J. R.; Border, J.; Rillema, D. P.; McCarthy, P.; Shields, G. D. *J. Inorg. Biochem.* **1982**, *16*, 47.
(6) Collman, J. P.; Gagñe, R. R.; Reed, C. A.; Robinson, W. T.; Rodley, G. A. *Proc. Natl. Acad. Sci. U.S.A.* **1974**, *71*, 1326.
(7) Baldwin, J. E.; Huff, J. *J. Am. Chem. Soc.* **1973**, *95*, 5757.
(8) Collman, J. P.; Gagñe, R. R.; Reed, C. A.; Halbert, T. R.; Lang, G.; Robinson, W. T. *J. Am. Chem. Soc.* **1975**, *97*, 1427.
(9) Hoffman, B. M.; Petering, D. H. *Proc. Natl. Acad. Sci. U.S.A.* **1970**, *67*, 637.
(10) Yonetani, T.; Yamamoto, H.; Woodrow, G. V. *J. Biol. Chem.* **1974**, *249*, 682.
(11) Schammel, W. P.; Mertes, K. S. B.; Christoph, G. G.; Busch, D. H. *J. Am. Chem. Soc.* **1979**, *101*, 1622.
(12) Kimura, E.; Sakanaka, A.; Makamoto, M. *Biochim. Biophys. Acta* **1981**, *678*, 172.
(13) Pasternack, R. F.; Halliwell, B. *J. Am. Chem. Soc.* **1979**, *101*, 1026.
(14) Pasternack, R. F.; Skowronek, W. R. *J. Inorg. Biochem.* **1979**, *11*, 261.
(15) Pasternack, R. F.; Banth, A.; Pasternack, J. M.; Johnson, C. S. *J. Inorg. Biochem.* **1981**, *15*, 261.
(16) Bailey, C. L.; Bereman, R. D.; Rillema, D. P.; Nowak, R. *Inorg. Chem.* **1984**, *23*, 3956.
(17) Bailey, C. L.; Bereman, R. D.; Rillema, D. P.; Nowak, R. *Inorg. Chem.* **1986**, *25*, 933.
(18) Lever, A. B. P.; Pickens, S. R.; Minor, P. C.; Licoccia, S.; Ramaswamy, B. S.; Magnell, K. *J. Am. Chem. Soc.* **1981**, *103*, 6800.
(19) Weiss, M. C.; Goedken, V. L. *J. Am. Chem. Soc.* **1976**, *98*, 3389.

0020-1669/86/1325-3149$01.50/0

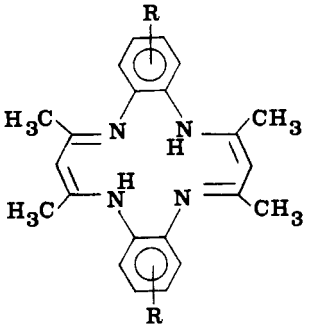

Figure 1. $[H_2Me_4(RBzo)_2[14]tetraeneN_4]$.

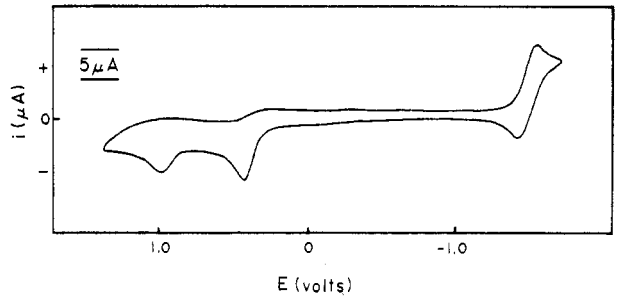

Figure 2. Cyclic voltammogram of $Cu[Me_4Bzo_2[14]tetraeneN_4]$ in a 0.10 M TBAH–CH_2Cl_2 solution. The scan rate was 200 mV/s and the potential was measured vs. SSCE.

included as supplemental material. All manipulations of cobalt(II) complexes were carried out in a rigorously dry and O_2-free atmosphere by utilizing a Vacuum Atmosphere Dri-Lab equipped with a Dri-Train.

Aldrich Gold Label acetonitrile and Fisher Spectraanalyzed methylene chloride were dried for 48 h over 4-Å molecular sieves and degassed with anhydrous N_2 before use. Pyridine was refluxed for 10 h over potassium hydroxide and distilled at atmospheric pressure under nitrogen. All other solvents were reagent grade and used without further purification. Tetraalkylammonium salts were purchased from Southwestern Analytical Chemicals, Inc., dried overnight at 70 °C under vacuum, and used without further purification.

Physical Measurements. Elemental analyses were performed by Atlantic Microanalytical Services. Electronic absorption spectra were obtained in either acetonitrile or methylene chloride solutions by using matched 1-cm or 0.1-cm quartz cells and were recorded with a Cary 14 spectrophotometer. ESR spectra were recorded with either a JEOL Model PE-1X spectrometer or a Varian E-3 spectrometer. The g values were measured relative to diphenylpicrylhydrazyl (DPPH), $g = 2.0036 \pm 0.0003$.

Cyclic voltammetric measurements were carried out as previously described.[16] *IR* compensation was used. Tetraethylammonium perchlorate (TEAP) and tetrabutylammonium hexafluorophosphate (TBAH) were used as electrolytes. Controlled-potential electrolysis experiments were carried out in the Vacuum Atmosphere Dri-Lab and were effected with a PAR 173 potentiostat and a PAR 176 coulometer. A three-electrode system was employed, consisting of a Pt-wire-mesh working electrode, a Pt-wire counter electrode and a Pt-wire reference electrode.

The cobalt(II) complexes and all oxidized or reduced complexes were sealed in spectral cells and quartz ESR tubes just prior to their removal from the dry box. "H" cells containing the cobalt(II) complexes were prepared inside the Dri-Lab, tightly sealed, and removed from the Dri-Lab, and cyclic voltammetry measurements were run vs. SSCE for direct comparison to measurements on copper(II) and nickel(II) analogues. The SSCE electrode was placed in the cell side arm that was isolated from the main compartment by a fine frit. No noticeable interferences from air were noted. Cobalt(II) complexes in ESR tubes were oxygenated with air at $T \geq -78$ °C with use of a dry ice–2-propanol slush in order to insure exposure to dioxygen at a low temperature.

Generation of superoxide $[O_2^-]$ was accomplished by controlled-potential electrolysis of oxygen-saturated acetonitrile solutions containing 0.10 M TEAP as electrolyte,[20] and superoxide concentrations were determined by measuring the absorbance at 40.0×10^3 cm^{-1} ($\epsilon = 1460$ M^{-1} cm^{-1}).

(20) Ozawa, T.; Hanaki, A.; Yamamoto, H. *FEBS Lett.* **1977**, *74*, 99.

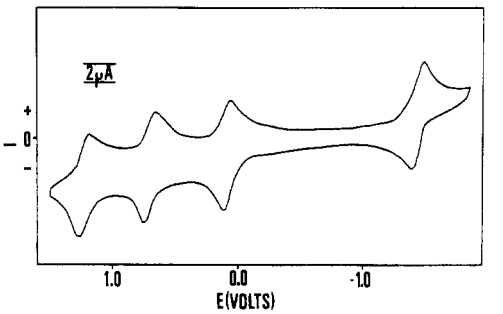

Figure 3. Cyclic voltammogram of $Co[Me_4(CO_2CH_3Bzo)_2[14]tetraeneN_4]$ in a 0.10 M TEAP–CH_3CN solution. The scan rate was 200 mV/s and the potential was vs. SSCE.

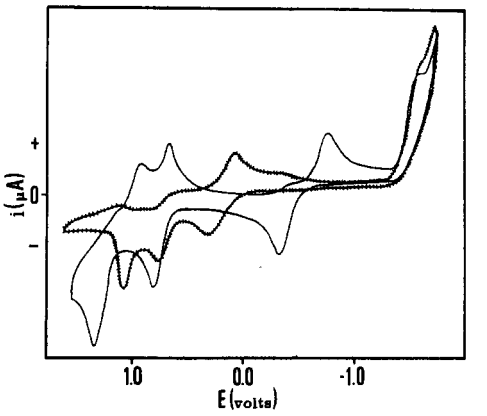

Figure 4. Cyclic voltammogram of $Co[Me_4(CO_2CH_3Bzo)_2[14]tetraeneN_4]$ in a 0.10 M TEAP–CH_2Cl_2 solution (+++) and in a 0.10 M TBAH–CH_2Cl_2 solution containing 10% pyridine (—). The scan rate was 200 mV/s and the potential was vs. SSCE.

Films of the copper(II) tetraazaannulene complex, $Cu[Me_4Bzo_2-[14]tetraeneN_4]$, were prepared by oxidative electropolymerization during repetitive scanning from +1.2 to −1.5 V vs. SSCE in methylene chloride solutions containing 1×10^{-3} M $Cu[Me_4Bzo_2[14]tetraeneN_4]$ and 0.10 M TBAH as the supporting electrolyte as previously described for nickel(II) tetraazaannulene films.[17]

Results

Electrochemistry. The electrochemical behavior of both copper complexes was similar to that of the nickel analogues in that two irreversible ligand-based oxidations and a reversible reduction associated with the metal center were observed (Figure 2). However, the positions of the cyclic voltammetric waves had changed as indicated by the potentials given in Table I. The oxidation waves were about 100 mV more negative and the reversible reduction waves were about 300 mV more positive for the copper complexes than for analogous nickel species. The positions of the waves of copper complexes were also solvent-dependent. In acetonitrile, the oxidation waves were about 100 mV less positive and the reduction waves were about 50 mV more positive than in methylene chloride. Controlled-potential electrolysis of $Cu[Me_4Bzo_2[14]tetraeneN_4]$ in methylene chloride 200 mV beyond the first oxidation waves and 200 mV beyond the reduction wave yielded n values of 0.95 and 1.02, respectively. Prior to electrolysis, the color of the solution was green. After electrolysis the color of the oxidized solution was orange and the reduced solution was yellow.

The electrochemical behavior of the cobalt(II) tetraazaannulenes in acetonitrile was unique in comparison to that observed for the copper and nickel analogues. As shown in Figure 3, the redox processes, including the two ligand-based oxidations and a metal-centered oxidation, exhibit reversible behavior. The additional oxidation wave at 0.01 V vs. SSCE corresponds to the Co(III/II) couple. The difference in peak potentials, ΔE_p, for all three oxidations were in the 60–70 mV range, a value consistent with theory for a reversible, one-electron-transfer processes; however, ΔE_p increased to about 90 mV for the reduction process

Table I. Electrochemical Data for $M[Me_4(RBzo)_2[14]tetraeneN_4]$ (R = H, CO_2CH_3) Complexes[a]

	oxidn potential,[b] V			redcn potential,[b] V
	$M^{II}L \rightarrow M^{III}L$	$ML \rightarrow M(L)^+$	$M(L)^+ \rightarrow M(L)^{2+}$	$M^{II}L \rightarrow M^{I}L$
$Cu[Me_4Bzo_2[14]tetraeneN_4]$				
CH_2Cl_2–0.1 M TBAH		0.46	1.00	−1.46 (60)
AN–0.1 M TEAP		0.37	0.87	−1.39 (60)
$Cu[Me_4(CO_2CH_3Bzo)_2[14]tetraeneN_4]$				
CH_2Cl_2–0.1 M TBAH		0.61	1.13	−1.22 (90)
AN–0.1 M TEAP		0.54	1.05	−1.17 (60)
$Co[Me_4Bzo_2[14]tetraeneN_4]$				
CH_2Cl_2–0.1 M TBAH	0.14 (140)	0.76	1.09	
AN–0.1 M TEAP	0.01 (60)	0.55 (60)	1.04 (60)	−1.65 (90)
$Co[Me_4(CO_2CH_3Bzo)_2[14]tetraeneN_4]$				
CH_2Cl_2–0.1 M TBAH	0.13 (120)	0.84	1.20	
AN–0.1 M TEAP	0.05 (60)	0.67 (60)	1.21 (65)	−1.45 (80)
$Ni[Me_4Bzo_2[14]tetraeneN_4]$[c]				
CH_2Cl_2–0.1 M TBAH		0.49	1.16	
AN–0.1 M TEAP		0.45	1.00	−1.73 (60)
$Ni[Me_4(CO_2CH_3Bzo)_2[14]tetraeneN_4]$[c]				
CH_2Cl_2–0.1 M TBAH		0.63	1.28	
AN–0.1 M TEAP		0.59	1.19	−1.51 (60)

[a] Volts vs. SSCE. Scan rate = 200 mV/s. [b] Numbers in parentheses refer to ΔE_p values. Absence of a value indicates the wave was irreversible. [c] See ref 16.

Table II. Electronic Absorption Bands for $M[Me_4(RBzo)_2[14]tetraeneN_4]$ (R = H, CO_2CH_3) Complexes[a]

	$\bar{\nu}_{max}$, 10^3 cm^{-1} (ϵ, M^{-1} cm^{-1})		$\bar{\nu}$, other transitions 10^3 cm^{-1} (ϵ, M^{-1} cm^{-1})	
complex	CH_2Cl_2	AN	CH_2Cl_2	AN
$Cu[Me_4Bzo_2[14]tetraeneN_4]$	15.85 (1200)	15.87 (810)	24.39 (10950)	24.51 (9600)
			26.60 (22500)	26.84 (18900)
			32.26 (10800)	32.79 (9900)
			35.46 (15500)	36.10 (15200)
			40.65 (23200)	41.32 (24100)
$Cu[Me_4(CO_2Bzo)_2[14]tetraeneN_4]$	15.70 (1300)	15.67 (800)	23.53 (10800)	23.53 (7500)
			25.77 (19300)	26.04 (12600)
			32.47 (15900)	32.26 (12700)
			40.98 (21700)	41.67 (17500)
$Co[Me_4Bzo_2[14]tetraeneN_4]$	17.21 (8210)	17.30 (7375)	18.66 (8190)	18.80 (7290)
			18.48 (12390)	18.52 (11030)
			24.33 (9280)	24.45 (14070)
			26.60 (19290)	27.17 (20340)
			31.15 (22370)	32.26 (26200)
$Co[Me_4(CO_2CH_3Bzo)_2[14]tetraeneN_4]$	16.69 (9930)	16.83 (9210)	21.28 (13200)	21.28 (13640)
			23.09 (14900)	23.36 (15100)
			25.91 (20320)	26.45 (27980)
			29.85 (20980)	30.03 (17770)
			37.04 (22210)	37.74 (17000)
$Ni[Me_4Bzo_2[14]tetraeneN_4]$[b]	17.09 (6300)	17.15 (6250)	25.38 (23600)	26.54 (36250)
			26.74 (15500)	26.81 (20000)
			30.03 (6700)	29.94 (7500)
			30.96 (6600)	37.74 (27100)
			37.45 (22900)	43.68 (27500)
$Ni[Me_4(CO_2CH_3Bzo)_2[14]tetraeneN_4]$[b]	16.84 (9900)	16.89 (8700)	22.73 (20100)	23.53 (24500)
			24.15 (22900)	37.74 (40000)

[a] Spectra were obtained by using 10^{-4} M solutions. [b] Reference 16.

assigned as the Co(II/I) couple. Quasi-reversible behavior is expected for redox couples that change coordination numbers in their two oxidation state forms.

The electrochemical behavior in methylene chloride was quite different, as shown in Figure 4a. The Co(III/II) couple now becomes quasi-reversible (ΔE_p = 140 mV) and the ligand-based oxidation waves also become irreversible as found in the nickel(II) and copper(II) complexes. Addition of pyridine to the methylene chloride solution failed to induce the reversible electrochemical behavior found in acetonitrile solutions (Figure 4b), indicating that the presence of a coordinating ligand does not account for the reversibility observed for the Co(II) complexes in acetonitrile. In addition, cyclic voltammograms obtained in DMF with 0.1 M TEAP as supporting electrolyte were similar to those obtained in 0.1 M TBAH–CH_2Cl_2 solutions, indicating that the reversibility in CH_3CN is most likely a solvent effect. Controlled-potential electrolysis of $Co[Me_4Bzo_2[14]tetraeneN_4]$ in acetonitrile 200 mV beyond the first oxidation wave and 200 mV beyond the reduction wave yielded n values of 0.98 and 0.95, respectively. The red color of the cobalt(II) solution changed to pinkish orange upon oxidation and green upon reduction. Cyclic voltammograms run after electrolysis were similar to those obtained before electrolyses.

Comparison of the M(II/I) potentials for the parent complexes indicated that the potentials fell in the order Cu(II) > Co(II) > Ni(II). The ligand-based oxidations followed the order Co > Ni > Cu. Thus, oxidations and reductions shifted in different orders, due possibly to the intervening Co(III/II) redox couple.

Electronic Spectra. Visible and ultraviolet data covering the range 11 × 10^3 to 40 × 10^3 cm^{-1} have been summarized in Table II. A comparison of absorption maxima in both acetonitrile and methylene chloride indicated a weak solvent dependence with the energy maxima falling at slightly higher energies in acetonitrile. The lowest energy visible transition has previously been assigned as a ligand to metal change transfer (LMCT)[16] and within each

Table III. ESR Parameters for O_2 Adducts of Cobalt(III) Complexes[a]

complex	$g_\perp$[b]	$g_\parallel$[b]	$10^4 A_\perp$Co,[c] cm^{-1}	$10^4 A_\parallel$Co,[c] cm^{-1}	$10^4 A_\parallel$N,[c] cm^{-1}
Co[Me_4Bzo_2[14]tetraeneN$_4$]·py	2.252	2.0039[d]		89.73	14.10
Co[Me_4Bzo_2[14]tetraeneN$_4$]·py(O_2)	1.997	2.074	10.22	17.25	
Co[$Me_4(CO_2CH_3Bzo)_2$[14]tetraeneN$_4$]·py	2.208	2.021[d]		74.80	11.57
Co[$Me_4(CO_2CH_3Bzo)_2$[14]tetraeneN$_4$]·py(O_2)	1.998	2.086	8.95	18.68	

[a] Toluene–CH_2Cl_2 (1:1 v/v) solutions at 77 K. [b] Error is ±0.002, unless otherwise noted. [c] Error is ±1. [d] Error is ±0.0003.

ligand derivative series (R = H, R = CO_2CH_3), the energy maxima fell in the sequence Co(II) > Ni(II) > Cu(II). In addition, the LMCT energy maxima for the metallo complexes containing the ligand with the electron-withdrawing substituent R = CO_2CH_3 are found at lower energy than those with R = H. One point to note is the large difference in the molar absorptivity of the LMCT band between copper and the other two metal derivatives. Clearly, in the case of copper, the transition is less favorable.

After controlled-potential electrolysis, the electronic absorption spectra of the oxidation and reduction products were compared to that of the parent complex, Co[$Me_4(CO_2CH_3Bzo)_2$[14]tetraeneN$_4$]. The spectra consisted of a large number of intense charge-transfer transitions from the near-infrared region to the ultraviolet region. Upon reduction, the visible band at 16.8×10^3 cm^{-1} was red-shifted to 15.8×10^3 cm^{-1}. However, the opposite trend was observed upon oxidation: the LMCT band was blue-shifted to 18.4×10^3 cm^{-1}.

Comparison of the electronic absorption spectrum of Cu[Me_4Bzo_2[14]tetraeneN$_4$] to that of the reduced complex indicated a loss of the visible absorption maximum at 15.6×10^3 cm^{-1} following reduction. Upon oxidation, the visible band was red shifted from 15.9×10^3 to 15.7×10^3 cm^{-1}.

Electron Spin Resonance. The ESR spectrum of the Cu[Me_4Bzo_2[14]tetraeneN$_4$] obtained in a frozen methylene chloride–toluene glass at 77 K was typical of a copper(II)–N_4 environment with $g_\parallel = 2.155$ (±0.002) and $g_\perp = 2.056$ (±0.002). Following controlled-potential electrolysis 200 mV beyond the first oxidation wave, an ESR signal with g values 2.149 (±0.002) and 2.045 (±0.002), respectively, was obtained. Clearly the metal species in solution was still copper(II). This is explained by coupling of ligand-based radicals to form dimeric species as outlined in eq 1.[17] As expected, the reduced copper complex was

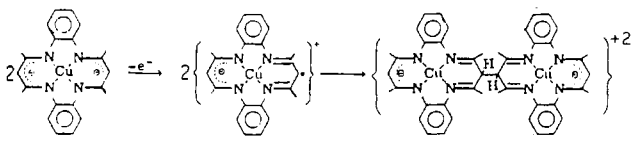

(1)

diamagnetic due to formation of a d^{10} copper(I) species.

In determining the reactivity of Cu(II) complexes with superoxide, both the spin-Hamiltonian parameters and the optical data for Cu[Me_4Bzo_2[14]tetraeneN$_4$] following successive additions of superoxide ion were tabulated. Addition of superoxide ion (1:1) resulted in a doubling of the molar absorptivity, followed by a gradual decrease in successive additions, with the value never reaching that of the original complex. However, the ESR parameters remained virtually unchanged following successive additions of superoxide, with only slight changes being observed for both the g and A values.

The ESR spectra of Co[Me_4Bzo_2[14]tetraeneN$_4$] and Co[$Me_4(CO_2CH_3Bzo)_2$[14]tetraeneN$_4$] were typical of coblat(II) macrocycles. Both complexes exhibited broad, ill-defined spectra in neat solvents, but in the presence of an axial base, such as pyridine, they gave spectra consistent with five-coordinate cobalt(II) (see Figure 6 in supplementary material). The cobalt(III) complex generated by controlled-potential electrolysis was ESR silent, as expected, but the second oxidized product did yield an isotopic ESR signal, with a g value of 2.0027 consistent with a cobalt(III)–ligand radical structure. Addition of oxygen to five-coordinate pyridine adducts at low temperature (−78 °C) resulterd in formation of a six-coordinate cobalt(III) superoxide derivative, as indicated by the ESR specturm (see Figure 7 in supplementary material). The ESR parameters for the five-coordinate pyridine adducts and the superoxide species are given in Table III. The five-coordinate pyridine complexes exhibited $g_\perp > g_\parallel$ and $A_\parallel$ values between 75×10^{-4} and 90×10^{-4} cm^{-1}, while six-coordinate superoxide adducts exhibited $g_\perp < g_\parallel$, while $A_\parallel^{Co}$ values decreased to approximately 20×10^{-4} cm^{-1}.

Discussion

Visible–UV Spectra. Lever et al.[18] have developed a model for analyzing charge-transfer spectra on the basis of redox potentials. The model relates the energy of the transition to the difference in redox potential between that of the metal and of the ligand. A linear correlation (correlation coefficient = 0.995) is observed between the energy of the lowest visible absorption band maximum and the difference between the peak potential for ligand oxidation and the potential for metal reduction in nickel, cobalt, and copper tetraazaannulenes, suggesting these are LMCT in nature. The remaining electronic transitions correlate with the type of ligand derivative. For example, for R = CO_2R, the nickel(II), copper(II) and cobalt(II) complexes exhibit complementary bands at 23.5 $\times 10^3$, 23.5 $\times 10^3$, and 23.4 $\times 10^3$ cm^{-1}, respectively, while parent (R = H) complexes have an analogous set at 25.6 $\times 10^3$, 24.5 $\times 10^3$, and 24.5 $\times 10^3$ cm^{-1}, respectively. The only exception to these intraligand absorptions is an additional visible transition for each cobalt(II) complex with an absorption maximum at 18.8 $\times 10^3$ cm^{-1} (R = H) and 21.3 $\times 10^3$ cm^{-1} (R = CO_2CH_3). The additional absorptions are most likely ligand to metal charge-transfer (LMCT) transitions, similar in assignment and origin to the first LMCT but to a higher energy d level. This intermediate LMCT band is present in all the cobalt complexes, regardless of their oxidation states. However, the energy maxima for both the first and second LMCT band shift in accord with the oxidation state of the cobalt and the maxima fall in the expected order of Co(III) > Co(II) > Co(I).

Electrochemistry. The redox properties of a number of transition-metal complexes based on H_2[$Me_4(RBzo)_2$[14]tetraeneN$_4$] have been investigated. The most detailed studies were carried out with complexes of nickel,[21,22] rhodium,[23,24] rhenium,[23,24] and palladium.[24] In most cases, irreversible ligand oxidations were observed; however, in the case of rhodium and rhenium carbonyl dimers [$Rh(CO)_2$]$_2$$Me_4Bzo_2$[14]tetraeneN$_4$ and [$Re(CO)_3$]$_2$$Me_4Bzo_2$[14]tetraeneN$_4$, the first oxidation was reversible. In addition, Dabrowiak has reported evidence for reversibility of the first ligand oxidation wave for the nickel complex using ac polarography.[21] Perhaps the most unusual of the series studied so far has been the reversibility found for Co[Me_4Bzo_2[14]tetraeneN$_4$] in acetonitrile as previously illustrated (see Figure 3). The cyclic voltammogram was unusual in the sense that all redox processes including two ligand oxidations were reversible. The reason for reversible vs. irreversible redox behavior of the ligand may be related to the degree of metal–ligand electronic interactions. For the cobalt case, the molecular orbitals that describe the metal–ligand electronic interactions may provide a mechanism that stabilizes the ligand free radical formed upon oxidation. The mechanism may invovle stabilization due to the higher positive

(21) Dabrowiak, J. C.; Fisher, D. P.; McElroy, F. C.; Macero, D. J. *Inorg. Chem.* **1979**, *18*, 2304.
(22) McElroy, F. C.; Dabrowiak, J. C. *J. Am. Chem. Soc.* **1976**, *98*, 7112.
(23) Kadish, K. M.; Bottomley, L. A.; Schaeper, D.; Tsutsui, M.; Bobsein, R. L. *Inorg. Chim. Acta* **1979**, *36*, 219.
(24) Kadish, K. M.; Schaeper, D.; Bottomley, L. A.; Tsutsui, M.; Bobsein, R. L. *Inorg. Nucl. Chem.* **1980**, *42*, 469.

charge (+3 for cobalt) or the metal center may act as an electron sink equilibrating the electron distribution through the whole molecule. Evidence for greater metal–ligand interaction can be noted from data in Table II, where the molar absorptivity for the LMCT transition is lowest for the copper complex and the largest for the cobalt complex.

Superoxide Adducts. The formation of superoxide adducts of cobalt(III) tetraazaannulenes was postulated by Goedkin and co-workers,[19] but positive evidence regarding their existence was not presented. The results reported here indicate, at low temperature and in the presence of an axial base, addition of dioxygen to the cobalt(II) tetraazaannulene complexes resulted in the formation of six-coordinate cobalt(III) superoxide adducts. The ESR parameter for both the five-coordinate pyridine adducts and the six-coordinate superoxide species were similar to those found for five-coordinate Co(II) and superoxide adducts of cobalt(III) porphyrins.[25,26]

Previously it had been shown that a linear correlation existed between the Co(III/II) redox couple and the ability of a complex to bind dioxygen.[27] The relationship was based on redox couples determined in neat pyridine. Examination of the redox behavior of Co[Me_4Bzo_2[14]tetraeneN$_4$] in neat pyridine indicated that the Co(III/II) couple was irreversible. The reduction occurred at $E_p = -0.92$ V, while the oxidation peaked at $E_p = -0.27$ V vs. SSCE. The irreversibility was probably related to a rapid change from a six-coordinate bis(pyridine) adduct for the Co(III) complex to a five-coordinate one upon reduction back to a Co(II) species. However, the reduction potential was quite negative, suggesting that the complex would bind dioxygen very strongly. As expected, exposure of a 10% pyridine–methanol solution containing 1×10^{-4} M Co[Me_4Bzo_2[14]tetraeneN$_4$] in a low-temperature optical cell[28] at −78 °C to O_2 (0.5 Torr) resulted in an immediate disappearance of the 16.3×10^3 cm^{-1} band of the Co(II) complex and the appearance of a 18.3×10^3 cm^{-1} absorption band characteristic of a Co(III) species. Unfortunately, the spectral change was irreversible (e.g. in vacuo), indicating that, even at −78 °C, the O_2^- intermediate only had a transient lifetime and the species continued to react to produce a Co^{III}[Me_4Bzo_2[14]tetraeneN$_4$]·2py$^+$ adduct.

Experimental evidence supporting formation of the Cu^{II}·O_2^- adduct is based on spectral and electrochemical evidence. As noted in the results section, the molar absorptivity value doubled upon addition of a stoichiometric quantity of O_2^- to Cu[Me_4Bzo_2-[14]tetraeneN$_4$] in acetonitrile. This suggests that a 1:1 Cu(II):O_2^- adduct has formed, as outlined in eq 2. Continued addition of

$$\text{Cu[Me}_4\text{Bzo}_2\text{[14]tetraeneN}_4\text{]} + O_2^- \rightarrow \{O_2^-\cdot\text{Cu[Me}_4\text{Bzo}_2\text{[14]tetraeneN}_4\text{]}\} \quad (2)$$

O_2^- resulted in a slow decrease in the absorbance at 15.63×10^3 cm^{-1} and in a small decrease in the intensity of the EPR signal. The origin of this effect is unknown but it may be due to formation of a bis(superoxo) species or to formation of Cu(I). Valentine and co-workers[29] observed a more dramatic EPR signal intensity change for a saturated macrocyclic ligand copper(II) complex when the superoxide to copper(II) ratio was greater than 1:1 and attributed the decrease to deprotonation of the ligand.

The spectral data suggesting the interaction of O_2^- with Cu-[Me_4Bzo_2[14]tetraeneN$_4$] are supported by the catalytic reduction of O_2 and O_2^- at electropolymerized films of {Cu[Me_4Bzo_2[14]-tetraeneN$_4$]}$_n$ on a platinum electrode. In Figure 5a, the electrochemical response of the O_2/O_2^- couple at a bare Pt electrode has been compared to the same process at a Pt electrode modified with an electropolymerized {Cu[Me_4Bzo_2[14]tetraeneN$_4$]}$_n$ film

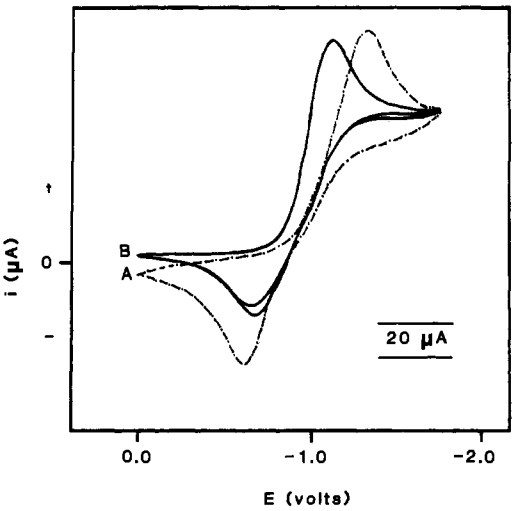

Figure 5. Cyclic voltammogram of O_2-saturated solutions containing 0.10 M TEAP–CH_3N for a bare platinum electrode (-··-) and for a platinum electrode modified with {Cu[Me_4Bzo_2[14]tetraeneN$_4$]}$_n$ by oxidative electropolymerization (—).

(Figure 5b). The catalytic nature of the film has been indicated by a more favorable O_2/O_2^- reduction potential, which shifts 70 mV from that observed for a bare Pt electrode. Furthermore, the diminished current observed for the reoxidation of O_2^- indicates a loss of redox equivalents when compared to the bare electrode case. The loss in equivalents is probably due to reduction of Cu(II) in the film to Cu(I), which then transfers its electron to O_2^- forming O_2^{2-} and Cu(II). Thus, the electrode functions catalytically by two mechanisms. The Cu(II) initially coordinates O_2, weakly facilitating its reduction to O_2^-, and then upon its reduction to Cu(I) at a more negative potential, further reduces O_2^- to O_2^{2-}. Reportedly, activation of O_2 at surface-modified electrodes containing metallophthalocyanines involves initial formation of superoxide species followed by electrochemical reduction to peroxides.[30]

We are currently studying the details of both catalytic O_2 and CO_2 reduction at surface-modified electrons of metallotetraazaannulenes.

Acknowledgment. This work was supported by the Office of Naval Research and the North Carolina Biotechnology Center. D.P.R. thanks the National Science Foundation for a Dri-lab Grant No. CHE-8312663. This is paper No. 8 from the North Carolina Biomolecular Engineering and Materials Application Center.

Registry No. Cu[Me_4Bzo_2[14]tetraeneN$_4$], 56285-38-2; Cu-[Me_4Bzo_2[14]tetraeneN$_4$]$^+$, 103190-80-3; Cu[Me_4Bzo_2[14]tetraeneN$_4$]$^{2+}$, 103190-84-7; Cu[Me_4Bzo_2[14]tetraeneN$_4$]$^-$, 103190-88-1; Cu-[$Me_4(CO_2CH_3Bzo)_2$[14]tetraeneN$_4$], 103190-77-8; Cu[Me_4-($CO_2CH_3Bzo)_2$[14]tetraeneN$_4$]$^+$, 103190-81-4; Cu[Me_4-($CO_2CH_3Bzo)_2$[14]tetraeneN$_4$]$^{2+}$, 103190-85-8; Cu[Me_4-($CO_2CH_3Bzo)_2$[14]tetraeneN$_4$]$^-$, 103190-89-2; Co[Me_4Bzo_2[14]tetraeneN$_4$], 60193-64-8; Co[Me_4Bzo_2[14]tetraeneN$_4$]$^+$, 103190-82-5; Co-[Me_4Bzo_2[14]tetraeneN$_4$]$^{2+}$, 103190-86-9; Co[Me_4Bzo_2[14]tetraeneN$_4$]$^-$, 103190-90-5; Co[$Me_4(CO_2CH_3Bzo)_2$[14]tetraeneN$_4$], 103190-78-9; Co[$Me_4(CO_2CH_3Bzo)_2$[14]tetraeneN$_4$]$^+$, 103190-83-6; Co[Me_4-($CO_2CH_3Bzo)_2$[14]tetraeneN$_4$]$^{2+}$, 103190-87-0; Co[Me_4-($CO_2CH_3Bzo)_2$[14]tetraeneN$_4$]$^-$, 103190-91-6; Co[Me_4Bzo_2[14]tetraeneN$_4$]·py, 66303-87-5; Co[Me_4Bzo_2[14]tetraeneN$_4$]·py(O_2), 103200-97-1; Co[$Me_4(CO_2CH_3Bzo)_2$[14]tetraeneN$_4$]·py, 103190-79-0; Co[Me_4-($CO_2CH_3Bzo)_2$[14]tetraeneN$_4$]·py(O_2), 103200-98-2; {Cu[Me_4Bzo_2-[14]tetraeneN$_4$]}$_n$, 103190-93-8; {Cu[Me_4Bzo_2[14]tetraeneN$_4$]}$_2^{2+}$, 103190-92-7; Pt, 7440-06-4; O_2, 7782-44-7; O_2^-, 11062-77-4.

Supplementary Material Available: Table of elemental analyses of carbon, hydrogen and nitrogen and frozen-glass ESR spectra of the Co(II) (Figure 6) and Co(III) (Figure 7) complexes (3 pages). Ordering information is given on any current masthead page.

(25) Walker, F. A. *J. Am. Chem. Soc.* **1970**, *92*, 4235.
(26) Drago, R. S.; Beugelsdijk, T.; Breese, J. A.; Cannady, J. P. *J. Am. Chem. Soc.* **1978**, *100*, 5374.
(27) Carter, M. J.; Rillema, D. P.; Basolo, F. *J. Am. Chem. Soc.* **1974**, *96*, 392.
(28) Wicker, C. M., Jr.; Morgen, R. D.; Rillema, D. P. *J. Phys. Chem.* **1983**, *87*, 5151.
(29) Nappa, M.; Valentine, J. S.; Miksztal, A. R.; Schugar, H. J.; Isied, S. S. *J. Am. Chem. Soc.* **1979**, *101*, 7744.
(30) Zagal, J. H.; Paez, M.; Sturum, J.; Ureta-Zannartu, S. *J. Electroanal. Chem. Interfacial. Electrochem.* **1984**, *181*, 295.